HYPERDIFFUSION, MAXIMUM ENTROPY PRODUCTION, AND THE SIMULATED EQUATOR-POLE TEMPERATURE GRADIENT IN AN ATMOSPHERIC GENERAL CIRCULATION MODEL

Author: Axel Kleidon
Department of Geography and
Earth System Science Interdisciplinary Center
2181 Lefrak Hall
University of Maryland
College Park, MD 20742
USA

e-mail: akleidon@umd.edu
phone: 301-405-3203
fax: 301-314-9299

Working Paper
"01-Hyperdiffusion.pdf"

deposited on the Digital Repository at the University of Maryland
http://drum.umd.edu

1/10/05

ABSTRACT. Hyperdiffusion is used in atmospheric General Circulation Models to account for turbulent dissipation at subgrid scale and its intensity affects the efficiency of poleward heat transport by the atmospheric circulation. We perform sensitivity simulations with a dynamic-core GCM to investigate the effects of different intensities of hyperdiffusion and different model resolutions on the simulated equator-pole temperature gradient. We examine the different simulations using entropy production as a measure of baroclinic activity and show that there is a maximum in entropy production. In comparison to the climate at a state of maximum entropy production, every other simulated climate at a given resolution leads to an increased equator-pole temperature gradient. We then demonstrate that maximum entropy production can be used to tune low-resolution models to closely resemble the simulated climate of a high-resolution simulation. We conclude that tuning a GCM to a state of maximum entropy production is an efficient tool to tune low-resolution climate system models to adequately simulate the equator-pole temperature gradient.

INTRODUCTION

The equator-pole temperature gradient (DTEP) is of central importance to the global climate system. The gradient is affected by the strength of the atmospheric circulation, which compensates to some extent for the differences in radiative forcing by transporting heat. Paleoclimatological indicators suggest that DTEP has changed significantly in the past due to differences in the radiative forcing. For instance, for warm climates during the Eocene and the Cretaceous, atmospheric concentrations of carbon dioxide were significantly higher, and resulted in a much reduced temperature gradient of 19-23 K in comparison to today's value of about 33 K (Pierrehumbert, 2002). On the other hand, during ice ages of the Pleistocene, the temperature gradient was increased to 50 K. Clearly, the snow albedo feedback and cloud feedbacks add to the causes for the difference in radiative forcing. Here, however, we solely focus on the role of the atmospheric circulation in transporting heat and how it is represented by atmospheric General Circulation Models (GCMs).

The transport of heat by the atmospheric circulation requires work. Kinetic energy is dissipated by boundary layer friction, so that it requires continuous input of work to maintain the atmospheric circulation. This work is derived from the temperature gradient that develops between the tropics and the poles from the different amounts of radiation received. When this source of available potential energy (APE) is converted into motion, it results in the transport of heat to the poles. To a large extent, the heat transport is performed by the turbulent mixing of air masses in the mid-latitudes by baroclinic activity, which leads to the production of entropy and a reduction of DTEP, and therefore the source of APE.

It has been hypothesized that the atmospheric circulation does not dissipate energy at any rate, but at the maximum possible rate (Lorenz 1960). Closely related, it has been suggested that the atmospheric circulation adjusts to a state of maximum entropy production (e.g. Paltridge 1975, 1978; Grassl 1981; Ozawa et al. 2003; Kleidon et al 2003; Ito and Kleidon 2004). At this state, both, the rate of generation of available potential energy and the rate of dissipation by boundary layer friction are maximized. Studies with energy balance models have demonstrated that the resulting equator-pole temperature gradient associated with a MEP state is consistent with observations on Earth (e.g. Paltridge 1978) and other planetary bodies (Lorenz et al. 2001).

The maximum in entropy production can easily be demonstrated by simple considerations. Let us take the amount of heat transport from the tropics to the pole to be proportional to the temperature difference DTEP, multiplied with an effective conductivity k. Consider the case of $k = 0$: With no heat being transported, there would be no dissipation of heat by friction, and consequently no energy would be degraded, no work would be done by the atmospheric circulation and entropy production would be zero. At the other extreme of $k \rightarrow \infty$, there would be no temperature difference between the equator and the pole, therefore no available potential energy as a source to extract work, and consequently no entropy would be produced. Therefore, for an intermediate value of k, there must be a maximum in entropy production. The MEP hypothesis states is that the atmospheric circulation adjusts itself in steady state to maximize the rate of entropy production.

A recent theoretical advance has provided us with a foundation why a complex dynamic system, such as the Earth's atmosphere, should adjust to a MEP state (Dewar 2003, 2004). Dewar applied information theory to a non-equilibrium system and showed that if a system has sufficient degrees of freedom, a state of maximum entropy production is the most likely steady state of the system. In a recent paper we have applied Dewar's line of reasoning to simulations with a simple, dynamic core atmospheric General Circulation Model (Kleidon et al. 2003). Since there is no water or radiative transfer in this GCM, essentially all entropy produced in the model is due to the mixing of air masses of different temperatures in the mid-latitudes. Entropy production in this setup is therefore a direct measure of baroclinic activity. We argued that the model's spatial resolution constrains the spatial degrees of freedom of the atmospheric flow by imposing a limit on the minimum eddy size explicitly simulated in the dynamics, so that we should expect higher rates of entropy production with increasing model resolution. This was confirmed by the model simulations, in which we found that entropy production increases up to a spectral resolution of T42 after which entropy production is no further increased with increasing the model resolution. This would suggest that a model resolution of T42 would provide sufficient spatial degrees of freedom to the atmospheric flow in the context of the simple GCM used. We also showed with these simulations that the climate at a MEP state has profound climatological implications. Out of a range of model simulations of varying model resolution and intensities of boundary layer friction, the simulated climate leading to MEP is the one with the most effective heat transport, therefore exhibiting the smallest equator-pole temperature gradient.

The purpose of this paper is to extend the study of Kleidon et al. (2003) and investigate the role of hyperdiffusion in simulating the equator-pole temperature gradient. Hyperdiffusion is a parameterization used in GCMs to account for energy dissipation at small scales that are not resolved by the model. The intensity of hyperdiffusion in the GCM will clearly affect baroclinic activity and therefore entropy production. We should also expect that hyperdiffusion becomes less important with increasing model resolution, because a wider range of eddy sizes can be resolved in the model. In this sense, higher resolution simulations should provide us with insights whether

MEP states in low resolution models are realistic. We first demonstrate that there is a maximum in entropy production associated with a particular intensity of hyperdiffusion. Then we use the simulated climate of the MEP state as a reference climate and compare other sensitivity simulations to the MEP climate. We do this sensitivity analysis for different model resolutions so that we can explore whether the tuning of the model parameterization to MEP can be used to improve the accuracy of low-resolution models.

In the next section, we briefly describe the GCM used in this study and how we incorporated the diagnostic entropy production calculations into the model. We describe the simulation setup and the evaluation strategy. We then describe the simulations in terms of entropy production, zonal temperatures and its variability. We close with a brief discussion and conclusion.

METHODS

Puma-1 GCM

We use the PUMA-1 atmospheric GCM (Fraedrich et al. 1996). The PUMA-1 GCM is a simple, multi-level GCM (Hoskins and Simmons 1975; James and Gray 1986; James and James 1989; Held and Suarez 1994). It consists of the dynamical core of a GCM only, that is, there are no explicit calculations of the radiation or water balance. The dynamics of the atmosphere are forced by diabatic heating/cooling and by boundary layer friction, which appear as linear terms in the thermodynamic and momentum equations. The diabatic heating drives the atmospheric circulation by relaxing its temperature towards a radiative-convective equilibrium state on a time scale of τ_{HEAT} = 30 days for the upper layers, τ_{HEAT} = 10 days for the second-lowest model layer and τ_{HEAT} = 5 days for the lowest model layer. The effects of boundary layer turbulence and friction are modeled by Rayleigh friction in the lowest model layer, that is, $(u, v)/\tau_{FRIC}$ describes the deceleration of the air in the lowest model layer, with (u, v) being the horizontal wind speed components. We use a value of τ_{FRIC} = 3 days in T42 spectral resolution and five vertical layers of equal mass as our control simulation. This simulation leads to an atmospheric circulation close to MEP. Hyperdiffusion H for a climatic variable X in PUMA-1 is expressed as:

$$H(X) = K(-1)^h \nabla^{2h} X \tag{1}$$

where h is a constant (with a value of $h = 8$ in the PUMA-1 GCM), and K a characteristic hyperdiffusion constant ($K = 0.25$ day^{-1} in the control simulation). Hyperdiffusion is applied in spectral space to vorticity, divergence, and temperature. The model documentation and code is available for download at http://puma.dkrz.de.

Calculation of Entropy Production

We included diagnostic entropy production calculations into the GCM (Kleidon et al. 2003). For a parcel of air with a change in heat content dQ/dt at a temperature T, the flux of entropy F_σ, is calculated as:

$$F_\sigma \approx \frac{1}{T}\frac{dQ}{dt} \tag{2}$$

Here the approximation is made that the change of $1/T$ associated with the change in heat content is relatively small and can be neglected. The change in heat content dQ/dt is calculated for each grid box i and each model layer j by:

$$\frac{dQ_{i,j}}{dt}(t) = \frac{c_p}{g}\left(p_{i,j}^{t+\Delta t} \cdot T_{i,j}^{t+\Delta t} - p_{i,j}^{t-\Delta t} \cdot T_{i,j}^{t-\Delta t} \right) \cdot \Delta z_j \tag{3}$$

where the hydrostatic approximation is used to express the density of the air parcel (of temperature $T_{i,j}$ and pressure $p_{i,j}$), c_p is the specific heat capacity of air, g is the gravitational constant, Δz is the layer thickness in sigma coordinates, and the superscript referring to the respective values at previous time step $t - \Delta t$, the current time step t and the future time step $t + \Delta t$ (these values are available due to the numerical scheme used to integrate the equations of fluid dynamics). Entropy fluxes are then calculated by:

$$F_{\sigma,i,j}(t) = \frac{c_p}{g}\frac{\left(p_{i,j}^{t+\Delta t} \cdot T_{i,j}^{t+\Delta t} - p_{i,j}^{t-\Delta t} \cdot T_{i,j}^{t-\Delta t} \right)}{T_{i,j}^{t}} \cdot \Delta z_j \tag{4}$$

The global mean entropy production σ of the climatic mean state is then the global time average of

$F_{\sigma,i,j}$:

$$\sigma = \overline{\sum_{i,j} F_{\sigma,i,j}(t)} \tag{4}$$

In order to evaluate the effective temperatures at which the entropy production occurs, we sum up the positive and negative heat and entropy fluxes separately:

$$Q^{+} = \overline{\sum_{Q_{i,j}>0} Q_{i,j}(t)} \tag{5}$$

$$Q^{-} = \overline{\sum_{Q_{i,j}<0} Q_{i,j}(t)} \tag{6}$$

$$F_{\sigma}{}^{+} = \overline{\sum_{F_{\sigma,i,j}>0} F_{\sigma,i,j}(t)} \tag{7}$$

$$F_{\sigma}{}^{-} = \overline{\sum_{F_{\sigma,i,j}<0} F_{\sigma,i,j}(t)} \tag{8}$$

This allows us then to calculate the effective temperatures by:

$$T^{+} = \frac{Q^{+}}{F_{\sigma}{}^{+}} \tag{9}$$

$$T^{-} = \frac{Q^{-}}{F_{\sigma}{}^{-}} \tag{10}$$

Simulation Setup and Evaluation

We conduct a range of model simulations of varying model resolutions and different values of the hyperdiffusion time constant. In all simulations, we use a constant friction time constant of τ = 3 days that leads to MEP at T42 resolution. The simulations are conducted for 10 years using perpetual southern hemisphere winter conditions, with the first 2 years discarded to exclude spin-up effects. We use model resolutions of T10, T21, T31, T42, and T63 with hyperdiffusion time constants of 0.1, 0.25, 0.5, 1, 2.5, 5, and 10 days. The simulations are evaluated with respect to the global mean entropy production, zonal means of entropy fluxes and 900 hPa temperatures, and their

respective variances as indicators of climatic variability. Zonal means are interpolated to a common grid for comparison.

RESULTS AND DISCUSSION

Sensitivity of entropy fluxes and production to hyperdiffusion

Figure 1 shows global mean entropy production as a function of hyperdiffusion constant K for different model resolutions. A maximum is found in all simulations, with the maximum shifting to smaller values of K with increasing model resolution. For resolutions of T21 and higher, the maximum is around 2.5 mW m^{-2} K^{-1}, with slightly lower values for higher resolution. Since entropy production can be seen as a measure of baroclinic activity, Figure 1 demonstrates that hyperdiffusion can lead to a similar magnitude of baroclinic activity as in a higher resolution model for model resolutions of T21 and higher. The sensitivity of entropy production to the intensity of hyperdiffusion decreases with increasing model resolution. Both of these trends are to be expected, since with higher resolution, finer eddy sizes are explicitly resolved which would seem to reduce the need for a hyperdiffusion parameterization in the model.

The maximum in entropy production results from the two differing effects of hyperdiffusion on the effectiveness of turbulent mixing: (i) the magnitude of the heat flux itself, which increases with greater K and (ii) the temperature difference which drives turbulent mixing, which decreases with greater K. These trends are shown in Figure 2 for T21 resolution. What this means is that with greater heat fluxes, degradation of energy to lower temperatures is less effective due to the reduced temperature gradient which therefore results in the peak of entropy production. Note that values that are beyond the MEP peak imply that more heat is transported than the work that would be available through the degradation of the gradient. This implies that for values of K that are greater than the value resulting in MEP, gradients are likely to be destructed more quickly.

Figure 3 shows a frequency histogram of the globally averaged net instantaneous entropy flux for T21 resolution and three different values of hyperdiffusion. Other resolutions show a similar distribution (not shown). From Figure 3 it can be seen that the values of the instantaneous

flux shift towards more positive values, therefore leading to increasing entropy production in the climatological mean. For hyperdiffusion values greater than the one leading to MEP, the distribution is broadened with the peak being reduced and the tail of the distribution extending towards larger positive values. When the variability of net entropy fluxes is investigated, in terms of its variance, Figure 4 shows that variability increases with the strength of hyperdiffusion for the lower resolution versions. The higher resolution versions of T42 and T63 show a peak in variability for a value of hyperdiffusion which corresponds to the maximum in the mean while this is not the case for the lower resolution simulations.

The zonal mean fluxes of entropy are shown in Figure 5 for T21, T42, and T63 resolution. These figures show that the peak in net entropy fluxes occurs at a latitude of 60° on the winter hemisphere independent of model resolution and hyperdiffusion. The magnitude of this pattern, however, is strongly modulated by the value of hyperdiffusion.

Climatic consequences of non-MEP climates

The different magnitudes of entropy production reflect different levels of baroclinic intensity, and therefore different intensities of poleward heat transport. This has important consequences for the simulated DTEP. Figure 6 shows the difference in simulated 900 hPa temperatures of non-MEP climates in comparison to the simulated climate at MEP for three model resolutions. All simulated non-MEP climates generally show colder lower atmosphere temperatures in polar regions than the MEP climate of up to 6K with a trend towards warmer tropical temperatures by as much as 4K. For small values of K, the cold bias is largest for the T21 resolution (Fig. 6a), while the bias increases for greater values of K with higher model resolutions (Fig. 6b, c). This general polar cold bias is consistent with the results of sensitivity simulations with respect to boundary layer friction and model resolution (Kleidon et al. 2003).

MEP as a tuning tool

The results show that the state of MEP can be used as a reference climate. It exhibits a climate of highest baroclinic activity, the most effective heat transport to the pole, leading to the least

temperature gradient. In order to show that the MEP climate is not just a reference climate, but for a given resolution also the climate which closely resembles the characteristics of a high resolution simulation, the climates at MEP states associated with different resolutions are compared in Figure 7. Figure 7a shows that the MEP climates of different model resolutions show similar profiles of net entropy fluxes, in terms of the location of the peak and in terms of the magnitude, except for the lowest resolution T10 simulation. Taking the T63 model resolution as the most realistic setup, the magnitudes of net entropy fluxes at T21 and T31 are somewhat overestimated. The simulated equator-pole temperature difference for all simulations are close to the T63 simulated climate except T10 (Figure 7b), demonstrating that adjusting hyperdiffusion to a MEP climate can be used to tune a low resolution model. However, even though the bias in the equator-pole temperature difference can adequately adjusted, the models of lower resolution show a tendency of overestimating climate variability (Figure 7c).

SUMMARY AND CONCLUSION

We have shown with sensitivity simulations with respect to the hyperdiffusion parameterization in a GCM that there is a climate at which entropy production is maximized (a MEP climate). This maximum can be understood by the contrasting effects of increasing heat flux versus decreasing temperature difference with increasing strength of hyperdiffusion. The simulations show that in comparison to the MEP climate, the other simulations showed a general cold bias at the pole. Using MEP, the error at low resolution can be substantially reduced, but not entirely compensated. We also demonstrated that the value of the hyperdiffusion parameter leading to the MEP state is sensitive to model resolution. However, what we have not shown is how sensitive this tuning procedure is to the applied radiative forcing. This study provides an effective tuning methodology for Earth system Models of Intermediate Complexity (EMICs) to ensure an adequate simulation of the equator-pole temperature gradient (e.g. Claussen et al 2002), able to reduce the polar cold bias often found in GCMs.

ACKNOWLEDGMENTS.

This work was stimulated by the author's visit of Klaus Fraedrich's research group at the

University of Hamburg. The author thanks Klaus Fraedrich, Torben Kunz, and Frank Lunkeit for stimulating discussions and support with PUMA. The author gratefully acknowledges support by the National Science Foundation through grant ATM336555.

REFERENCES

Claussen M, Mysak LA, Weaver AJ, Crucifix M, Fichefet T, Loutre M-F, Weber SL, Alcamo J, Alexeev VA, Berger A, Calov R, Ganopolski A, Goosse H, Lohmann G, Lunkeit F, Mokhov II, Petoukhov V, Stone P, Wang Z (2002) Earth system models of intermediate complexity: closing the gap in the spectrum of climate system models. Clim Dyn 18: 579-586.

Dewar RC (2003) Information theory explanation of the fluctuation theorem, maximum entropy production, and self-organized criticality in non-equilibrium stationary states. J Physics A 36: 631-641.

Dewar RC (2004) Maximum entropy production and non-equilibrium statistical mechanics. in: Kleidon A, Lorenz R (eds) Non-equilibrium thermodynamics and the production of entropy: life, Earth, and beyond. Springer Verlag, in press.

Fraedrich K, Kirk E, Lunkeit F (1998) Portable University Model of the Atmosphere. DKRZ Report 16, Deutsches Klimarechenzentrum, Hamburg, Germany.

Grassl H (1981) The climate at maximum entropy production by meridional atmospheric and oceanic heat fluxes. Q J R Meteorol Soc 107: 153-166.

Held IM, Suarez MJ (1994) A proposal for the intercomparison of the dynamical cores of atmospheric general circulation models. Bull Amer Meteor Soc 75: 1825-1830.

Hoskins BJ, Simmons AJ (1975) A multi-layer spectral model and the semi-implicit method. Q J R Meteorol Soc 101: 637-655.

Ito T, Kleidon A (2004) Entropy production of atmospheric heat transport. in: Kleidon A, Lorenz R (eds) Non-equilibrium thermodynamics and the production of entropy: life, Earth, and beyond. Springer Verlag, in press.

James IN, Gray LJ (1986) Concerning the effect of surface drag on the circulation of a planetary atmosphere. Q J R Meteorol Soc 112: 1231-1250.

James IN, James, PM (1989) Ultra-low-frequency variability in a simple atmospheric circulation model. Nature 342: 53-55.

Kleidon A, Fraedrich K, Kunz T, Lunkeit F (2003) The atmospheric circulation at states of maximum entropy production. Geophys Res Lett 30(23): 2223.

Lorenz EN (1960) Generation of available potential energy and the intensity of the general circulation, *in:* Pfeffer RC (ed) Dynamics of Climate, Pergamon Press, Oxford, UK, 86-92,.

Lorenz RD, Lunine JI, Withers PG, and McKay CP (2001) Titan, Mars and Earth: Entropy

production by latitudinal heat transport. Geophys Res Lett 28: 415-418.

Ozawa H, Ohmura A, Lorenz RD, Pujol T (2003) The second law of thermodynamics and the global climate system – A review of the maximum entropy production principle. Rev Geophys 41: 1018.

Paltridge GW (1975) Global dynamics and climate - a system of minimum entropy exchange. Q J R Meteorol Soc 101: 475-484.

Paltridge GW (1978) The steady-state format of global climate. Q J Roy Met Soc 104: 927-945.

Pierrehumbert RT (2002) The hydrologic cycle in deep-time climate problems. Nature 419: 191-198.

FIGURE CAPTIONS:

FIGURE 1: Global entropy production as a function of hyperdiffusion constant *K* for different model resolutions.

FIGURE 2: Effective temperature difference (dotted line) and heat flux (dashed line) as a function of hyperdiffusion constant *K* for T21 resolution. For comparison, entropy production (solid line) is also shown (scale as in Figure 1).

FIGURE 3: Frequency histogram of the globally averaged net entropy flux for T21 resolution for different hyperdiffusion constants.

FIGURE 4: Variance of globally averaged net entropy flux as a function of hyperdiffusion constant *K* for different model resolutions.

FIGURE 5: Zonal mean entropy fluxes for different hyperdiffusion constants *K* and for (a) T21, (b) T42, and (c) T63 resolution.

FIGURE 6: Zonal mean 900 hPa temperature difference compared to simulated climate at maximum entropy production for different hyperdiffusion constants *K* and different model resolutions (a: T21; b: T42; c: T63).

FIGURE 7: Comparison of simulated zonal mean (a) entropy fluxes, (b) 900 hPa temperatures, and (c) temperature variance at states of maximum entropy production for different model resolutions.

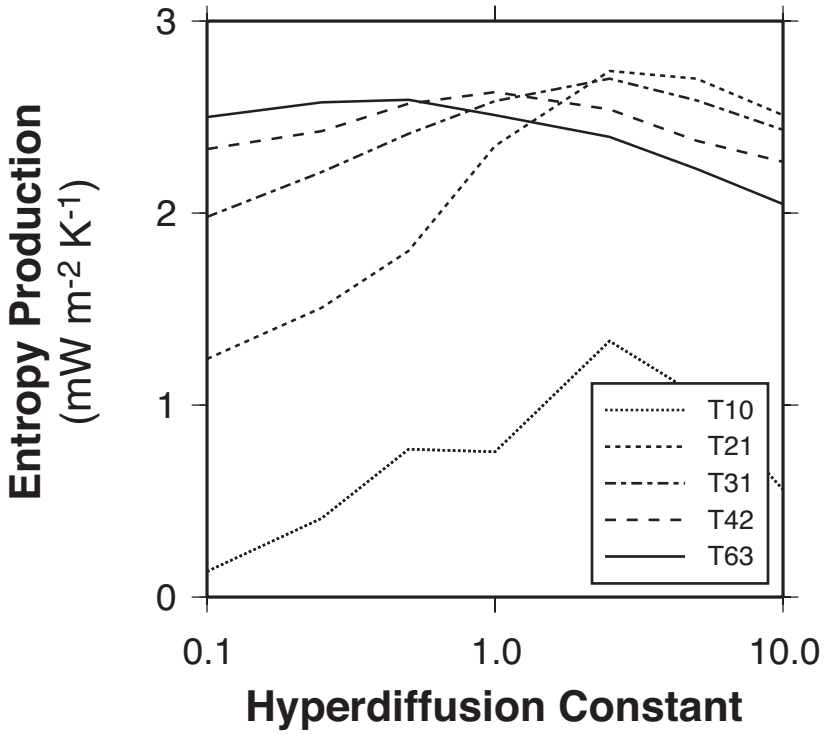

FIGURE 1: Global entropy production as a function of hyperdiffusion constant K for different model resolutions.

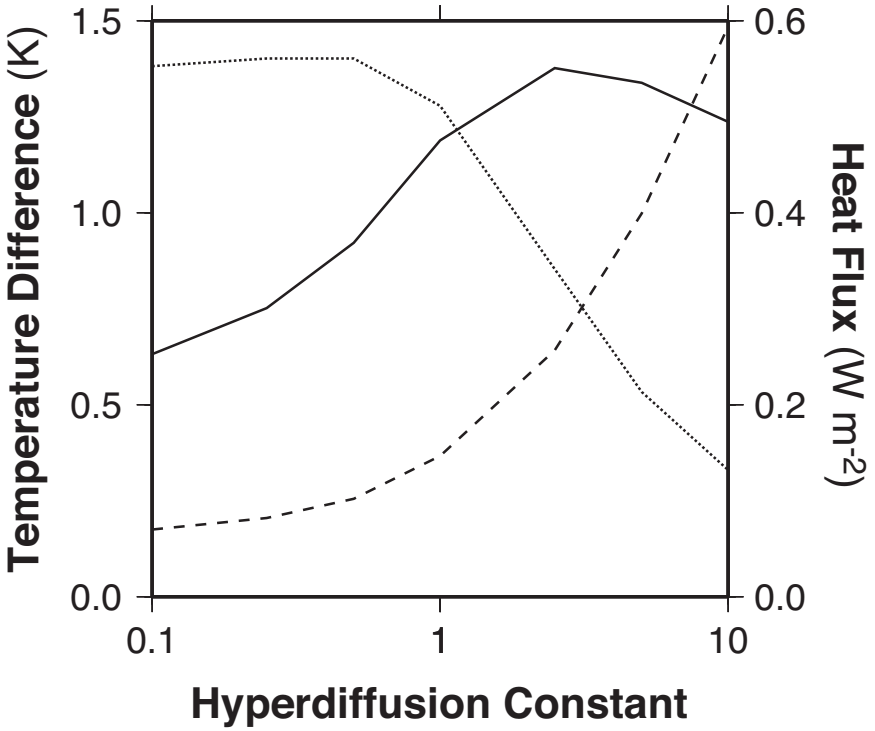

FIGURE 2: Effective temperature difference (dotted line) and heat flux (dashed line) as a function of hyperdiffusion constant K for T21 resolution. For comparison, entropy production (solid line) is also shown (scale as in Figure 1).

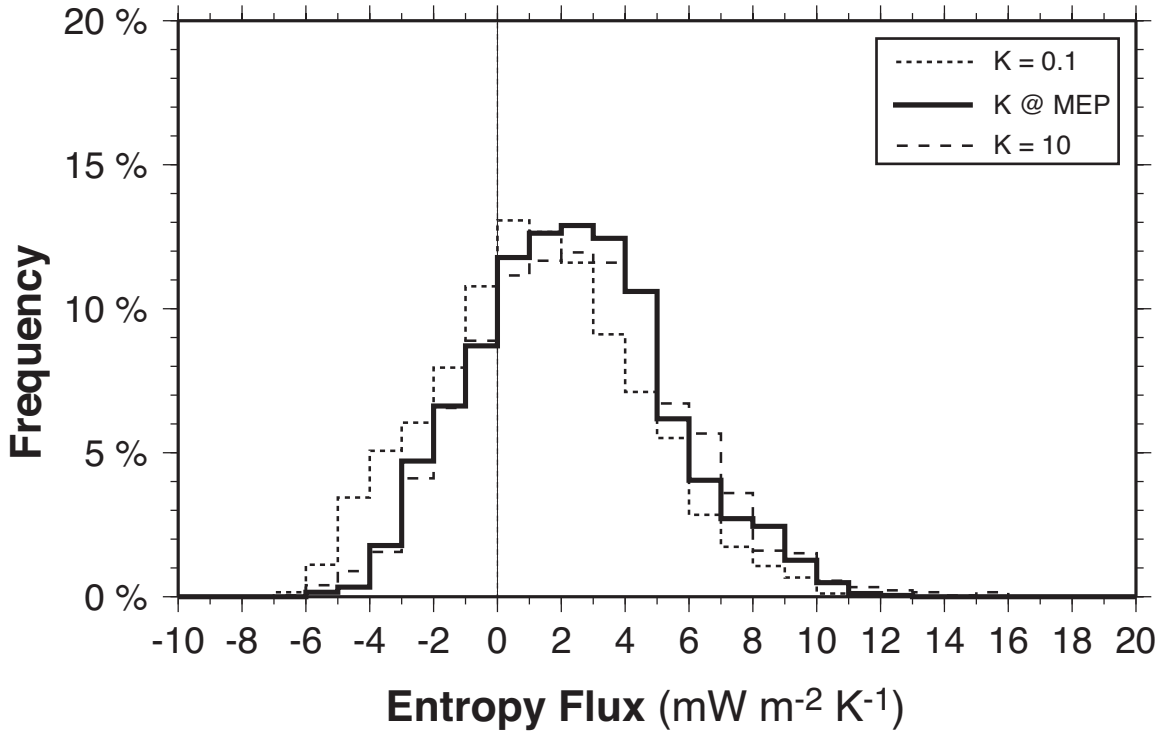

FIGURE 3: Frequency histogram of the globally averaged net entropy flux for T21 resolution for different hyperdiffusion constants.

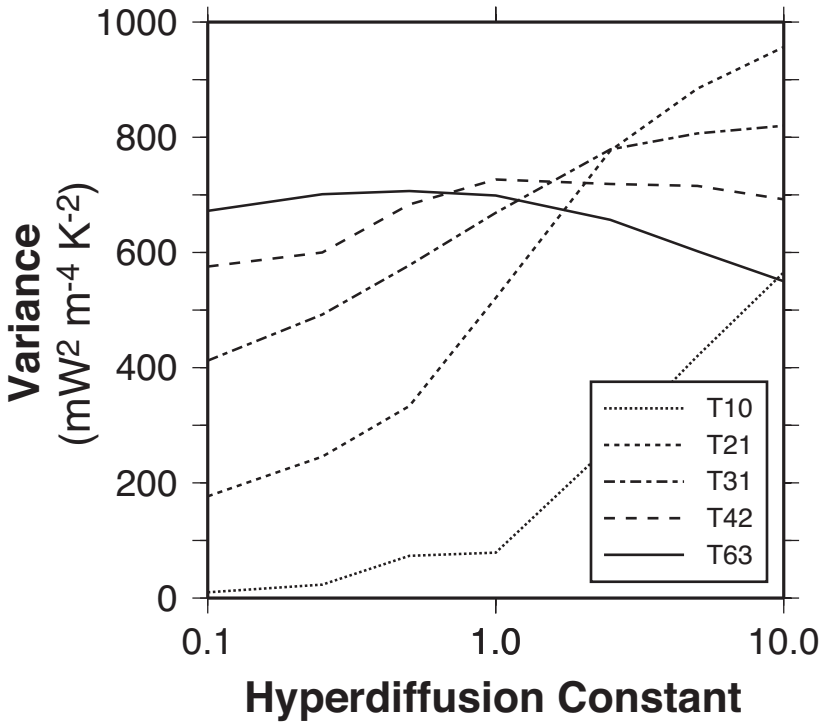

FIGURE 4: Variance of globally averaged net entropy flux as a function of hyperdiffusion constant *K* for different model resolutions.

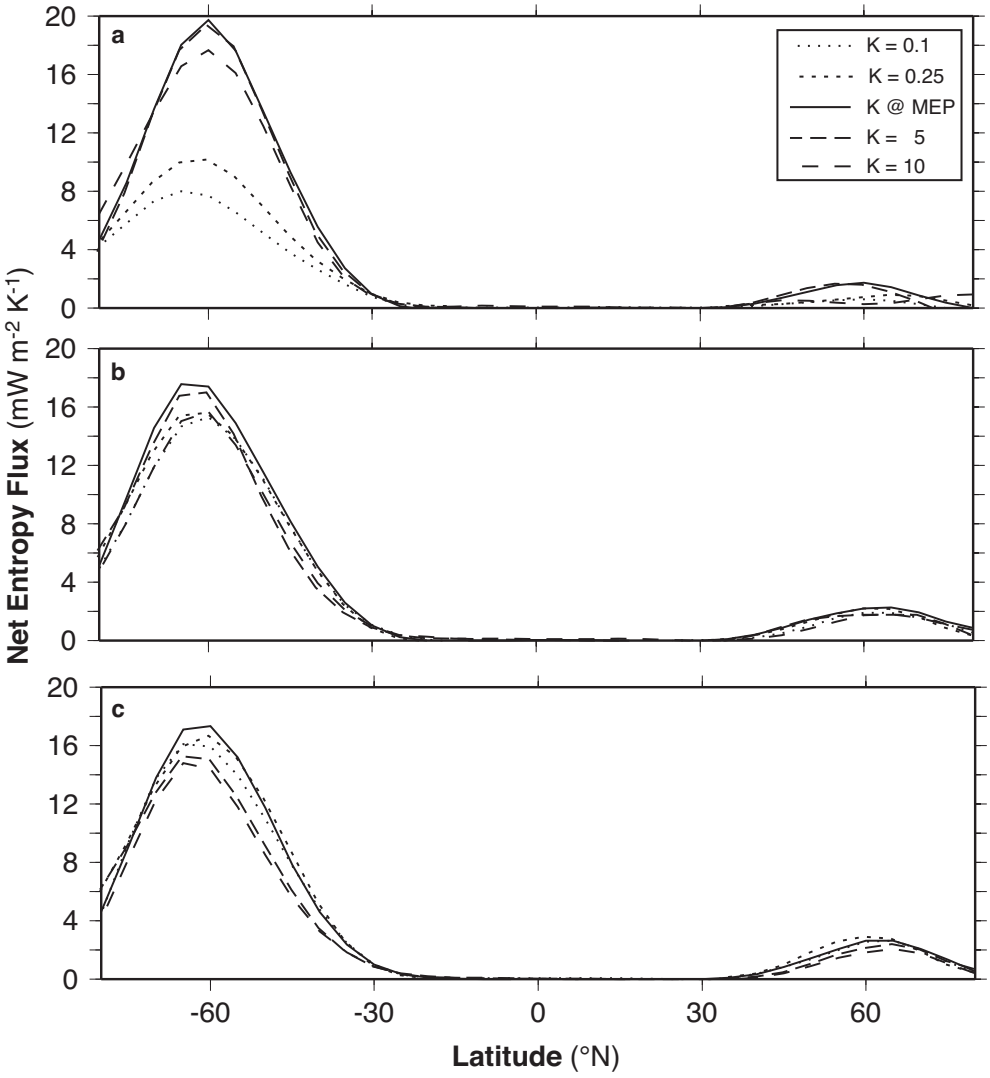

FIGURE 5: Zonal mean entropy fluxes for different hyperdiffusion constants K and for (a) T21, (b) T42, and (c) T63 resolution.

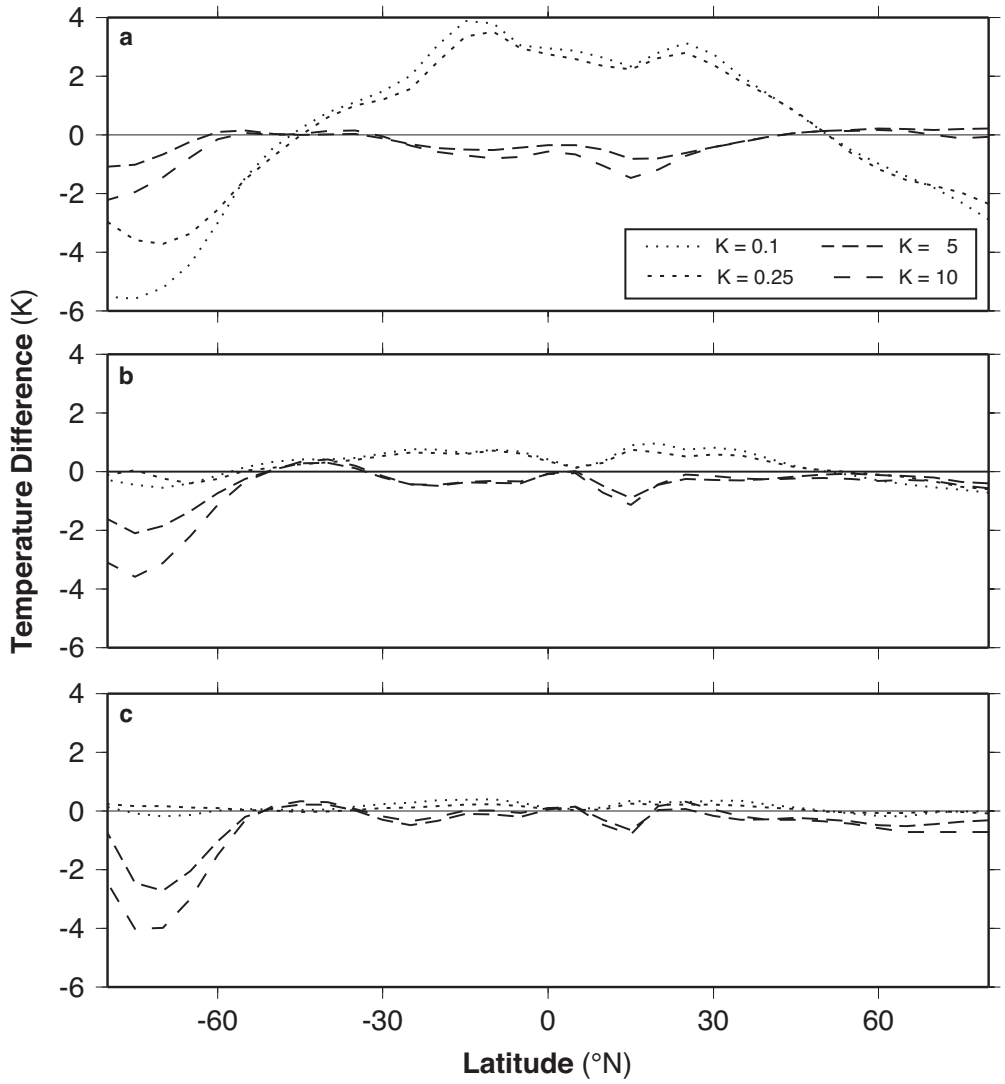

FIGURE 6: Zonal mean 900 hPa temperature difference compared to simulated climate at maximum entropy production for different hyperdiffusion constants K and different model resolutions (a: T21; b: T42; c: T63).

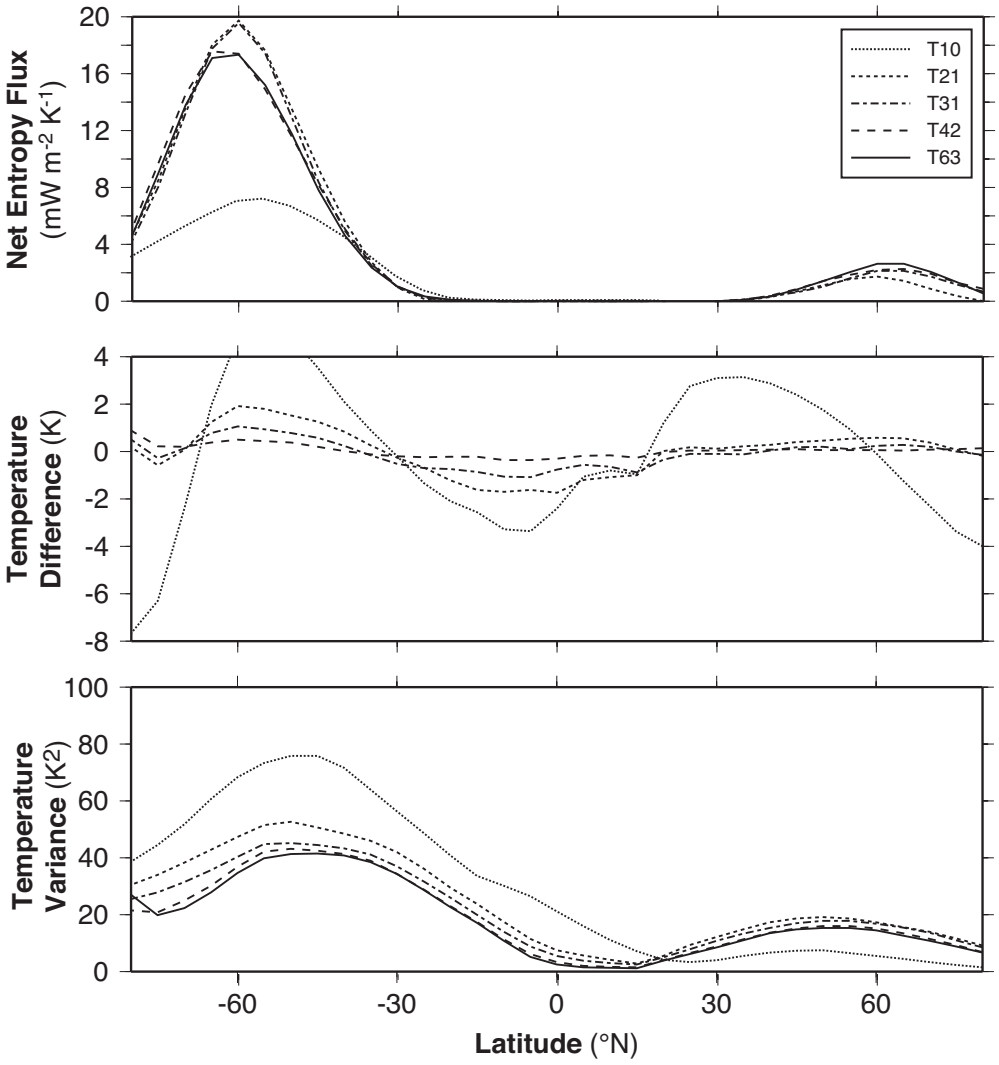

FIGURE 7: Comparison of simulated zonal mean (a) entropy fluxes, (b) 900 hPa temperatures, and (c) temperature variance at states of maximum entropy production for different model resolutions.